Wind and Structures, *Vol. 28, No. 5 (2019) 285-298*
DOI: https://doi.org/10.12989/was.2019.28.5.285

Numerical study on Reynolds number effects on the aerodynamic characteristics of a twin-box girder

Shujin Laima[*1,2,3], Buchen Wu[3], Chao Jiang[3], Wenli Chen[1,2,3] and Hui Li[1,2,3]

[1]*Key Lab of Smart Prevention and Mitigation for Civil Engineering Disasters of the Ministry of Industry and Information, Harbin Institute of Technology, Harbin 150090, China*
[2]*Key Lab of Structures Dynamic Behavior and Control of the Ministry of Education, Harbin Institute of Technology, Harbin 150090, China*
[3]*School of Civil Engineering, Harbin Institute of Technology, Harbin 150090, China*

(Received March 19, 2018, Revised August 2, 2018, Accepted August 17, 2018)

Abstract. For super long-span bridges, the aerodynamic forces induced by the flow passing the box girder should be considered carefully. And the Reynolds number sensitively of aerodynamic characteristics is one of considerable issue. In the study, a numerical study on the Reynolds number sensitivity of aerodynamic characteristic (flow pattern, pressure distribution and aerodynamic forces) of a twin-box girder were carried out using large eddy simulation (LES) with the dynamic Smagorinsky–Lilly subgrid model. The results show that the aerodynamic characteristics have strong correlation with the Reynolds number. At the leading edge, the flow experiences attachment, departure, and reattachment stages accompanying by the laminar transition into turbulence, causing pressure plateaus to form on the surface, and the pressure plateaus gradually shrinks. Around the gap, attributing that the flow experiences stages of laminar cavity flow, the wake with alternate shedding vortices, and turbulent cavity flow in sequence with an increase in the Reynolds number, the pressures around the gap vary greatly with the Reynold number. At the trailing edge, the pressure gradually recovers as the flow transits to turbulence (the flow undergoes wake instability, shear layer transition-reattachment station), In addition, at relative high Reynolds numbers, the drag force almost does not change, however, the lift force coefficient gradually decreases with an increase in Reynolds number.

Keywords: Reynolds numbers effects; LES; twin-box girder; pressure distribution; aerodynamic forces

1. Introduction

In recent decays, due to having better aeroelastic stability, steel twin-box girders have been widely adopted in super long-span bridges, for instance, the Xihoumen suspension Bridge in China (main span, 1650 m), Yi Sun-sin suspension Bridge in South Korea (main span, 1545 m), the Stonecutters' cable-stayed Bridge (main span, 1018 m), and so on. As well known, for these super long-span bridges, the wind-induced response is dramatic under the action of the aerodynamic forces. Therefore, the aerodynamic characteristics of the twin-box girder, which is induced by the flow passing the bluff body, should be considered carefully. For the flow passing the bluff body, the Reynolds number effect is an important issue. For instance, as the flow passes a circular cylinder, flow patterns, the drag force, lift force, and vortex-shedding frequency change with an increase in the Reynolds number (Williamson 1996, Zdravkovich 1997, Norberg 2003). In wind engineering, a common assumption is that the flow around box girder with sharp edges is independent of Reynolds number. However, more and more researches show that the Reynolds number effect is considerable for the box girders used in bridges. For the box girder of long-span bridges, the stream-wise aspect ratio (B/D, B and D are stream-wise width and depth of box girder respectively) is usually no less than 7. Due to the large aspect ratio, the flow firstly separates in the vicinity of the windward corner, and then transits into turbulence, eventually reattaches on the surface. The flow separation-reattachment process is very unsteady and have a strong correlation with the Reynolds number (Ota *et al.* 1981, Sasaki and Kiya 1991). In addition, the wake of the box girder also should have significant sensitivity to the Reynolds number as the wake of circular cylinder. Therefore, the Reynolds number effects may be a critical factor affecting the flow and aerodynamics characteristics of bridge decks.

The Reynolds number sensitively of box girders has received more and more attentions in recent years. Schewe and Larsen (1998) studied the Reynolds number effects on a bridge section at $1\times10^4 < \mathrm{Re} < 1\times10^7$ (the Reynolds number is based on the height of the bridge deck). To realize high Reynolds numbers, the experiment was carried out in a DLR high-pressure wind tunnel. The authors concluded that slender bodies with sharp edge cross-sections may suffer considerable Reynolds number effects owing to the topology variations of wake flow. Furthermore, Schewe (2001) pointed out that the Reynolds number effects on bluff bodies are due to the laminar separated shear layer transiting to turbulence. Larose and D'Auteuil (2006) summarized the researches about the Reynolds number sensitivity of the aerodynamics of bluff bodies with sharp edges and concluded that ignoring the Reynolds number effect on bluff bodies can lead to systematic errors. Larsen

[*]Corresponding author, Dr.
E-mail: laimashujin@126.com

http://www.techno-press.com/journals/was&subpage=7
ISSN: 1226-6116 (Print), 1598-6225 (Online)

et al. (2008) investigated the Reynolds number effects on mitigating the efficiency of vortex-induced vibration of a twin-box girder bridge using guide vanes. The authors concluded that the displacement thickness of the boundary layer must be less than 10% of the guide vane offset to allow for a sufficient flow rate to improve the efficiency of the guide vane in the prototype bridge. Zhang *et al.* (2008) investigated the vortex-induced vibration (VIV) of a twin-box girder at low and high Reynolds numbers. They found that the VIV existed in a broader range of damping ratios at low Reynolds numbers. Li *et al*. (2014) experimentally studied the flow passing over a twin-box girder and vortex-induced vibration at various Reynolds numbers, finding that the aerodynamic characteristics had significant Reynolds number effects due to the leading separation shear layers gradually transiting to turbulence. Furthermore, they found that the VIV of the twin-box girder with higher Reynolds number had higher critical reduced wind velocity, lager vibration amplitude, and larger lock-in range. Kargarmoakhar *et al*. (2015) experimentally investigated the effects of Reynolds number on the aerodynamic characteristics of a twin-deck bridge in the Re range of 1.3×10^6 to 6.1×10^6 based on the section width. The results show that the mean and fluctuating pressure distributions changed noticeably for zero and positive wind angles of attack while testing at different Re regimes. With the Re increase, a larger separation bubble formed on the bottom surface of the upstream girder accompanied with a narrower wake region, which causes drag coefficient decreased mildly and negative lift coefficient increased. Wang and Gu (2015) study the Reynolds number effects on the aerodynamic characteristics of rectangular prisms with various side ratios and rounded corners for Reynolds numbers ranging from 1.1×10^5 to 6.8×10^5. The results show that the sensitivity of aerodynamic behavior to the Reynolds number increases with increasing side ratio or rounded corner ratio for rectangular prisms.

In recent years, computational fluid dynamics (CFD) has become an important tool in bridge wind engineering. Kuroda (1997) numerically studied the flow over the box girder of the Great Belt East Bridge at Re $=3\times10^5$ with a 2-D laminar form in which the Reynolds number was based on the width of the box girder. Their simulated results indicated that the computed static force coefficients agreed well with wind tunnel test results, expect the lift force at the negative attack angle. Larsen and Walther (1997) simulated the flow past a cross section of a bridge girder and the corresponding flow-induced motions based on a 2-D discrete vortex method. Their results showed that the wind loads, flutter wind speed, and vertical vortex-induced response were in good agreement with wind tunnel test results. Bruno and Khris (2003) performed a computational study on evaluating the capability of 2-D numerical simulations to predict the vortical structures around the deck section of the Great Belt East Bridge. In general, the ensemble-averaged models of the turbulence did not properly simulate the small-scale complex eddies in the vortex-formation process. Watanabe and Fumoto (2008) studied the generation mechanism of the aerodynamic forces of a slotted box girder by large eddy simulation (Re = 1e4 based on the height of bridge deck). They found that the separation-reattachment phenomenon at the lower side of the leading edge of faring increases the drag and moment forces. Mannini *et al.* (2010) performed 2-D unsteady Reynolds-averaged Navier–Stokes simulations (URANS) of flow around inverted trapezoid cross-sections with lateral cantilevers of bridge decks at Re = [1.56e3 9.3e4] based on the height of bridge deck. They found that the Strouhal number increased and the mean drag decreased as the Reynolds number increased. Furthermore, their results showed that the presence of rounded corners increased the sensitivity of the bridge section to Reynolds number variations. Zhou and Ma (2010) Numerically studied the Reynolds number effect on flow around bluff body by deterministic vortex method (DVM) with Particle Strength Exchange (PSE). Numerical results show that the Reynolds number effect on aerostatic coefficients and Strouhal number of the bridges can not be neglected. In the range of the Reynolds number from 10^5 to10^6, it has great effect on the Strouhal number of Sutong Bridge, while the St is difficult to obtain from wind tunnel tests in this range. Nieto *et al.* (2010) carried out CFD simulations for the conceptual design of a 425 m length cable-stayed bridge are presented. According to these computations, the effect on the aerodynamic behavior of the deck cross-section caused by a number of modifications has been evaluated. And a new more feasible cross-section design has been proposed based on the CFD. Miranda *et al.* (2015) numerically studied the pressure distribution of a twin box girder deck with increasing the gap ratio by using the RANS and LES, and the simulation capability and limitation of RANS and LES were discussed in detail according to the experimental results. Dragomirescu *et al.* (2016) performed three-dimensional CFD simulations using a Large Eddy Simulation with a standard Smagorinsky subgrid-scale model, for Re = 9.3×10^7 and angles of attack α= -4°, -2°, 0°, 2° and 4°. The experimental and numerical results were compared with respect to accuracy, sensitivity, and practical suitability in the paper. Furthermore, the aerodynamic characteristics for each individual deck including static coefficients, wind flow pattern and pressure distribution were studied through CFD simulation.

Although there have been some advances in CFD application in aerodynamics of bridge decks, it is still very difficult to accurately simulate the aerodynamic performances and flow characteristics around the twin-box girder at various Reynolds numbers, owing to complicated aerodynamic configurations of bridge decks, which induces complicated flow dynamics issues, such as leading flow separation and reattachment, shear layer flow transition, the gap flow and so on. Therefore, the main goal of this study was to numerically investigate the Reynolds number effects on flow and aerodynamic characteristics of a twin-box girder in order to better understand the Reynolds number effects on the aerodynamic performances of bridge decks. It should be noted that another paper has been published (Laima *et al.* 2018), which mainly focused on the Reynolds number effects on the flow structures around the twin-box girder. However, for the paper, the Reynolds number sensitives of aerodynamic characteristics, such as pressure distributions and aerodynamic forces, are the main concerns. The structure of the paper is arranged as follows. In section 2, the numerical method and computational details are presented. In section 3, the simulation results are discussed in detail, including the Reynolds number effects on the flow patterns of a twin-box girder, the surface pressure distributions, and the aerodynamic force coefficients. Finally, conclusions are summarized.

2. Numerical simulation

2.1 Numerical method

Complicated unsteady flow separation and reattachment, and vortex shedding phenomenon occur when a fluid flows around a sharp-edge box girder with a gap. To accurately simulate the unsteady process of boundary layer separation and wake flow, and investigate the corresponding Reynolds number effects, a large eddy simulation (LES) was adopted to solve the Navier–Stokes (N–S) equation. LES directly solves the large eddies that represent three-dimension unsteady motions, where effects of small eddies that are smaller than grid spacing are resolved by the subgrid-scale stresses (SGS) model. The time-dependent filtered N–S formula is described below

$$\frac{\partial \bar{u}_i}{\partial x_i} = 0, \tag{1}$$

$$\frac{\partial \bar{u}_i}{\partial t} + \frac{\partial}{\partial x_j}\left(\bar{u}_i \bar{u}_j\right) = -\frac{\partial \bar{p}}{\partial x_i} + \frac{1}{\mathrm{Re}}\frac{\partial}{\partial x_j}\frac{\partial \bar{u}_i}{\partial x_j} - \frac{\partial \tau_{ij}}{\partial x_j}, \tag{2}$$

where i, j = 1.2.3, u_i are the velocity components along the Cartesian coordinates of x_i, t is the time, p is the pressure, Re is Reynolds number (Re= UD/v,), the overbar denotes the filtering operator, and τ_{ij} denotes the subgrid-scale stresses, which are defined by

$$\tau_{ij} = \overline{u_i u_j} - \bar{u}_i \bar{u}_j, \tag{3}$$

As the Boussinesq assumption states that the Reynolds stresses are proportional to the mean rate of strain, the subgrid-scale stresses can be expressed as

$$\tau_{ij} - \frac{1}{3}\tau_{kk}\delta_{ij} = -2v_{SGS}\bar{S}_{ij}, \tag{4}$$

$$\bar{S}_{ij} = \frac{1}{2}\left(\frac{\partial \bar{u}_i}{\partial x_j} + \frac{\partial \bar{u}_j}{\partial x_i}\right), \tag{5}$$

where v_{SGS} is the eddy viscosity of the subgrid-scale stress, the overbar presents filter operator, and $\bar{S}_{ij}$ is the filtered strain rate tensor.

Several eddy-viscosity models are widely used in the LES, such as the Smagorinsky model (Smagorinsky 1963), the dynamic Smagorinsky–Lilly model (Germano *et al*. 1991, Lilly 1992), and the wall-adapted local eddy-viscosity (WALE) model (Nicoud and Ducros 1999). In this study, to simulate the laminar transition, the dynamic Smagorinsky–Lilly model was adopted. The dynamic Smagorinsky–Lilly model can be expressed as follows

$$v_{SGS} = C\Delta^2\left|\bar{S}\right| \tag{6}$$

where Δ is the filter width, $\left|\bar{S}\right| = \left(2\bar{S}_{ij}\bar{S}_{ij}\right)^{1/2}$, and C is the Smagorinsky coefficient, which is determined as

$$C = \frac{1}{2}\frac{\langle L_{ij}M_{ij}\rangle}{\langle M_{ij}M_{ij}\rangle} \tag{7}$$

$$L_{ij} = -\bar{u}_i\bar{u}_j + \bar{u}_i\bar{u}_j \tag{8}$$

$$M_{ij} = -\tilde{\Delta}^2\left|\tilde{\bar{S}}\right|\tilde{\bar{S}}_{ij} + \Delta^2\left|\bar{S}_{ij}\right|\bar{S}_{ij} \tag{9}$$

in which, the overbar denotes test-filter operator, $\tilde{\Delta}$ is the test-filter width, which is twice filter width in the study, and $\langle\bullet\rangle$ denotes an averaging procedure.

All the quantities in Eqs. (1)-(9) are non-dimensionlized by the height of the twin-box girder D, the incoming free-stream velocity U_∞, and Re = $U_\infty D/v$. To figure out the flow and aerodynamic characteristics of a twin-box girder in a broad range of Reynolds number, twenty simulation cases, which are at Re = 2e2, 3e2, 5e2, 6e2, 8e2, 1e3, 2e3, 3e3, 4e3, 5e3, 6e3, 7e3, 8e3, 9e3, 1e4, 2e4, 4e4, 6e4, 8e4, 1e5, were carried out.

The simulations were carried out using the OpenFOAM C++ libraries, an open-source computational fluid dynamics package (http://www.openfoam.com). The finite volume method was used in the solver, and the pressure–velocity coupling was achieved with the pressure implicit with splitting of operators (PISO) method. The convection terms were discretized using the second-order linear-upwind stabilized transport (LUST) scheme. The Euler backward scheme was adopted for the temporal discretization. The calculations were carried out at the Grace High Performance Computing Facility of University College London (UCL) using 240 cores in parallel.

2.2 Computational domain and boundary conditons

Fig. 1 shows the detailed geometrical information of the investigated twin-box girder, which is composed of two parallel box girders with a gap of length L = 6 m, width B = 36 m and a center height of the bridge deck D = 3.51 m. The computational domain and corresponding boundary conditions are shown in Fig. 2. The inlet, outlet, top and bottom boundaries are 19D, 31D, 16D, and 16D away from the upstream twin- box girder surface, respectively, and the span-wise dimension of the computational domain is 1D (In the simulation, the effects of span-wise length was performed firstly. For the twin-box girder with span-wise length of 1D, the mean aerodynamic force coefficients are -0.199, 0.516, and -0.025 for the lift, drag and pitching moment, respectively. For the twin-box girder with span-wise length of 2D, the mean aerodynamic force coefficients are -0.195, 0.518, and -0.025, respectively. Comparing the simulation results of the two cases, it can be found that the aerodynamic forces are almost the same, which indicates that the span-wise dimension of D is enough for simulating the flow past the twin-box girders. Therefore, span-wise dimension of D is selected in the simulation model in the study.). On the surfaces of the bridge deck, the no-slip boundary condition was used. At the top and bottom walls of the computational domain, the free slip conditions were employed. For the span-wise direction, a periodical boundary condition was adopted. A steady uniform flow velocity was specified at the inlet boundary. And a convective boundary condition was used at the outlet.

2.3 Mesh and grid dependence

In the simulation, the hexahedral structured mesh was adopted, as shown in Fig. 3. To consider the grid size effect on the accuracy of the simulation, a preliminary grid dependence study was conducted for Re = 1e4 and 1e5. Table 1 summarizes aerodynamic forces, which indicates that Mesh A with a cell number of 2.8 million and Mesh B with a cell number of 13.7 million have adequate grid resolution in simulations at Re ≤ 1e4 and 1e4 < Re ≤ 1e5, respectively. Therefore, two kinds of mesh densities were adopted depending on the Reynolds number.

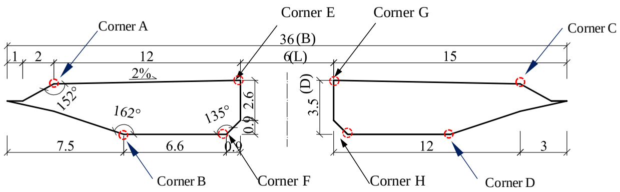

Fig. 1 Geometry details of the investigated twin-box girder (Unit: m)

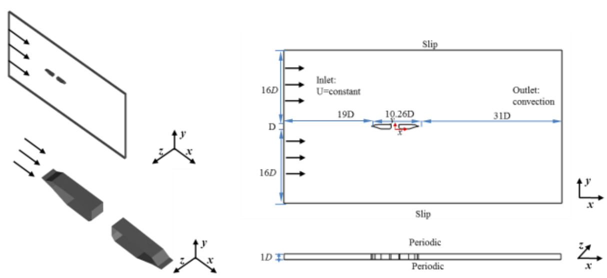

Fig. 2 Computational domain

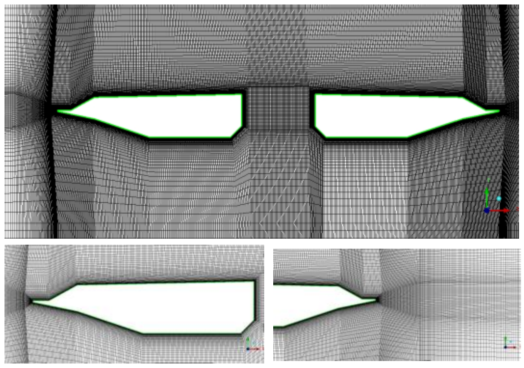

(a) Mesh A (2.8million cells)

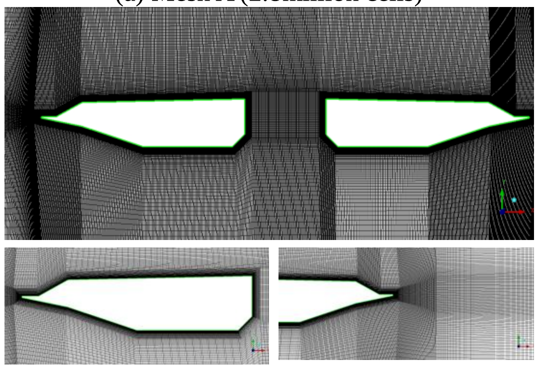

(b) Mesh B (13.7million cells)

Fig. 3 Section cut of the mesh around the twin-box girder

Table 1 The grid effect on the aerodynamic forces of a twin-box girder

Re	Mesh type	Cell number	Mean (C_d)	Mean (C_l)	Mean (C_m)
1e4	A	1.3 million	0.4813	-0.1638	-0.0290
		2.8 million	0.5156	-0.1988	-0.0245
		4.1 million	0.5188	-0.1949	-0.0245
1e5	B	9.2 million	0.4863	-0.1780	-0.0283
		13.7 million	0.4688	-0.1395	-0.0269
		16.3 million	0.4621	-0.1320	-0.0259

For Mesh A, the grid resolution on the surface of the twin-box girder was about $\Delta x/D \approx 2.25\text{e-}2$, $\Delta y/D \approx 2.30\text{e-}3$, $\Delta z/D \approx 4.56\text{e-}2$, and the corresponding mean wall $\Delta y^+ = 0.54$ at Re = 1e4 ($\Delta y^+ = u^*\Delta y/\nu$, where u* is the stream-wise friction velocity, Δy is the distance from fist node to the bridge surface $\Delta y+$. While for Mesh B, the grid resolution was about Δx/D ≈ 1.16e-2, $\Delta y/D \approx 1.14\text{e-}5$, $\Delta z/D \approx 4.56\text{e-}2$, and the corresponding mean wall $\Delta y^+ = 0.12$ at Re = 1e5. The auto time step with a courant number less than 1 was employed, and the mean dimensionless time $U\Delta t/D \approx 1.0\text{e-}3$ and 2.9e-4 for Re = 1e4 and 1e5, respectively.

2.4 Validation

To validate the large eddy simulation for flow around the twin-box girder, the aerodynamic forces and mean pressure coefficients on the surfaces were compared with the experimental results, which are shown in Figs. 4 and 5.

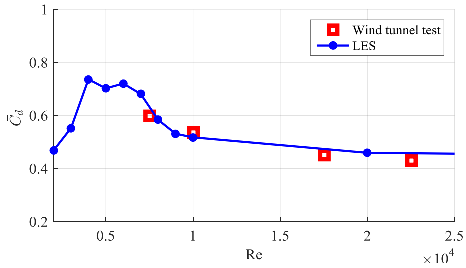

(a) Mean drag force coefficient

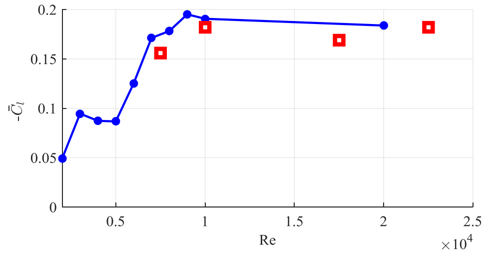

(b) Mean lift force coefficient

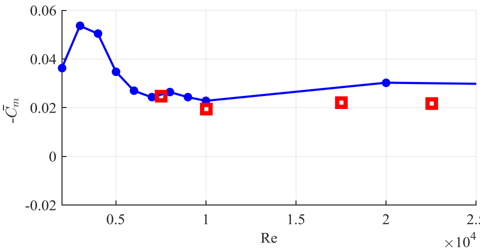

(c) Mean pitching moment coefficient

Fig. 4 Comparison of the aerodynamic forces and vortex shedding frequency obtained by LES and experiments

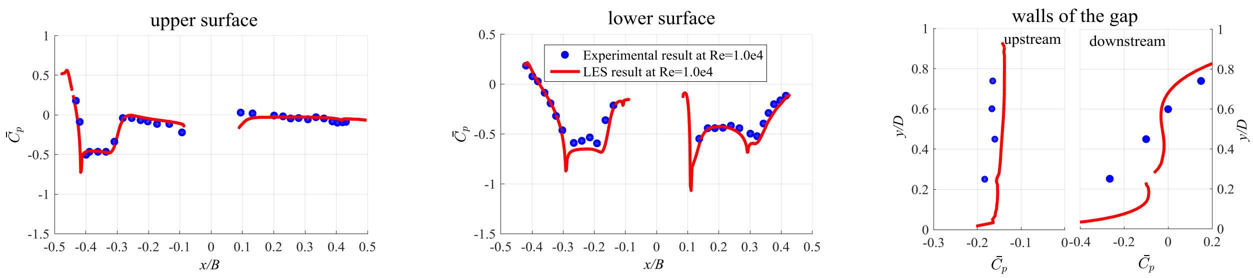

(a) Re = 1e4, experimental data from Chen *et al.* (2015)

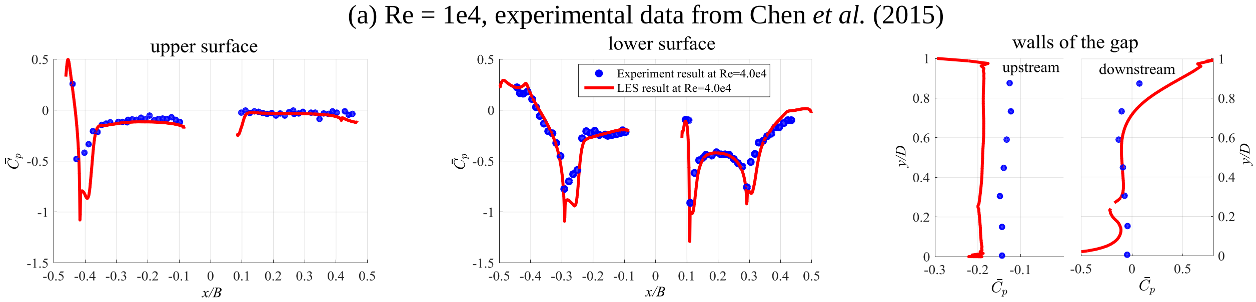

(b) Re = 4e4, experimental data from Li *et al.* (2014)

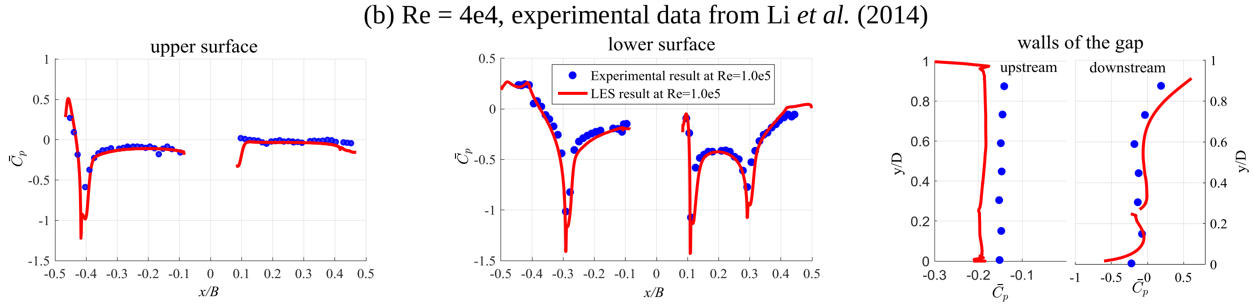

(c) Re = 1e5, experimental data from Li *et al.* (2014)

Fig. 5 Comparison of the aerodynamic forces and vortex shedding frequency obtained by LES and experiments

As the figures show, in general, the simulation results match considerably well with experimental results, although there are some discrepancies for mean pressure coefficients on walls of the gap, which may be attributed to the difference of the gap between the model used in the simulation and the one used in experiment. For the model of experiment, there are some connecting beams in the gap between the upstream and downstream box girder.

3. Results and discussions

3.1 Reynolds number effects on flow patterns

Flow motions around a sharp-edge box girder with a gap are complicated and have close correlation with the Reynolds number. Fig. 6 shows the instantaneous z-direction vorticity contours at z/D = 0.5 for Re = 2e2–1e7 based on the height of the twin-box girder. As Fig. 8 shows, the Reynolds number effect is significant.

At the leading edges, the flows experience attachment, departure, and reattachment stages depending on the Reynolds number, along with gradually transiting to turbulence. For 2e3 < Re ≤ 5e3, the laminar flow separates in the vicinity of the windward corner (Corner A and B), and then reattaches on the surface in a laminar state. The separation bubble length increases with the Reynolds number. While for 6e3 ≤ Re ≤ 8e4, the leading separated shear layer becomes unstable and transits to turbulence with the vortex shedding from the separating shear layer under the effect of Kelvin-Helmholtz (K-H) instability (Kiya and Sasaki 1985, Yang and Voke 2001), which results in the flow reattaching on the surface. The transition point gradually moves upstream with an increase in the Reynolds number. For Re > 8e4, the windward laminar boundary layers begin to transit to turbulence.

Around the gap, the flow goes through the following stages in sequence with an increase in the Reynolds number: closed cavity flow, laminar open cavity flow, a wake with alternate shedding vortices, and turbulent-open cavity flow. For Re < 2e3, the laminar shear layers on the top and bottom of the gap directly cross over the gap, which is similar to what occurs in closed cavity flow. At 2e3 < Re ≤ 5e3, the lower and upper shear layers become unstable, and the vortex impinges around the downstream corners (Corner G and H); the gap flow resembles laminar open cavity flow. At 5e3 < Re ≤ 8e3, the interaction between the upper and lower shear layers becomes considerable under the wake's global instability, resulting in the upper and lower shear layers rolling up alternately and large-scale vortices forming in the gap. This phenomenon is a typical feature of flow passing over a bluff body at a moderate Reynolds numbers, inducing alternately shedding vortex. Therefore, the gap flow can be considered as a wake flow model restricted by a downstream box girder. However, with further increases in the Reynolds number (Re > 8e3), owing to the effects of turbulent flow from the upstream box girder, the vortex formation length becomes longer at Re>8e3, inducing there is no enough space to form alternate shedding vortex in the gap. As a result, the phenomena characterized by the alternate rolling up of shear layers disappears.

In the wake of the downstream box girder, the flow undergoes stability, instability, and transition stations with an increase in the Reynolds number. For Re < 3e2, the wake is stable, with no vortex shedding. For 3e2 ≤ Re < 1e3, however, the wake becomes unstable, and regular Karman vortices appear in it. Furthermore, with an increase in the Reynolds number, the Karman Vortex gradually approaches the base of the twin-box girder. For higher Reynolds numbers, 1e3 < Re ≤ 2e3, the lower leeward shear layer transits into turbulence very quickly, and the regular Karman vortex disappears suddenly into the wake. For Re > 2e3, the shear layers gradually reattach on the trailing edge with an increase in the Reynolds number.

Fig. 7 shows the vortex structures around the bridge at some typical Reynolds numbers, where the vortex structure is obtained by the Lambda2 (λ2) criterion. As the figure shows, there are large number of vortices around the twin-box girder. As the Reynold number increases, the vortex is gradually distorted, resulting that the vortex becomes smaller and smaller, and the flows around the body transit to full turbulence.

3.2 Reynolds number effects on pressure distributions

Owing to the gradual transition of flows into turbulence, the pressure distributions on the surfaces of the stationary twin-box girder will have significant Reynolds number sensitivity. The pressure coefficient C_p is defined as

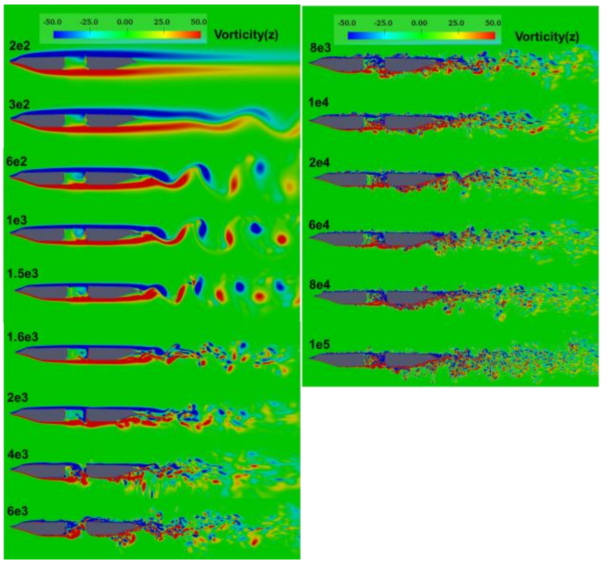

Fig. 6 Instantaneous z-direction (z/D = 0.5) vorticity contours at various Reynolds number

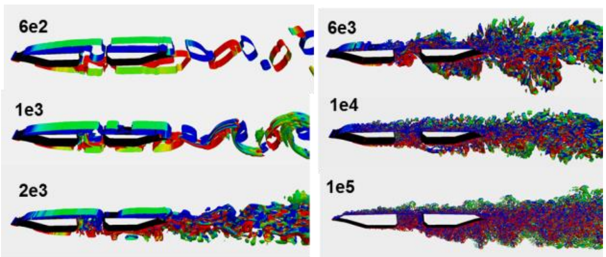

Fig. 7 Vortex structures at Re =6e3, 1e4, 1e5 (λ2 =-0.1, the vortex structures are colored by z-vorticity with the range of [-10 10])

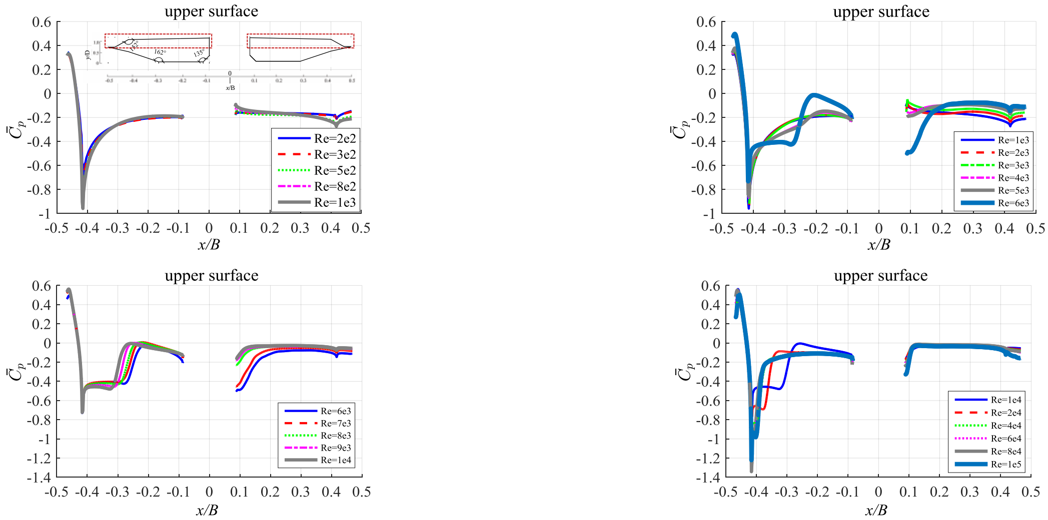

(a) Upper surface

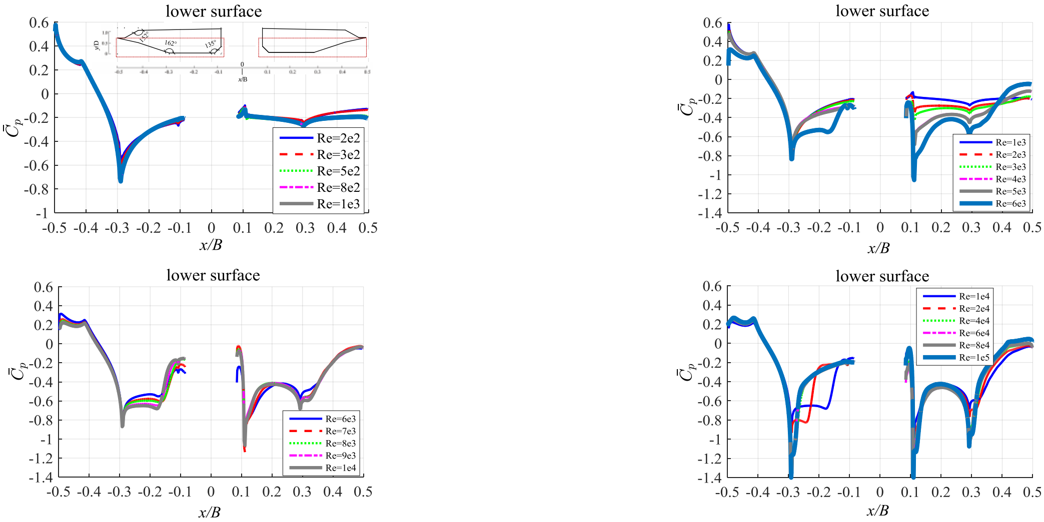

(b) Lower surface

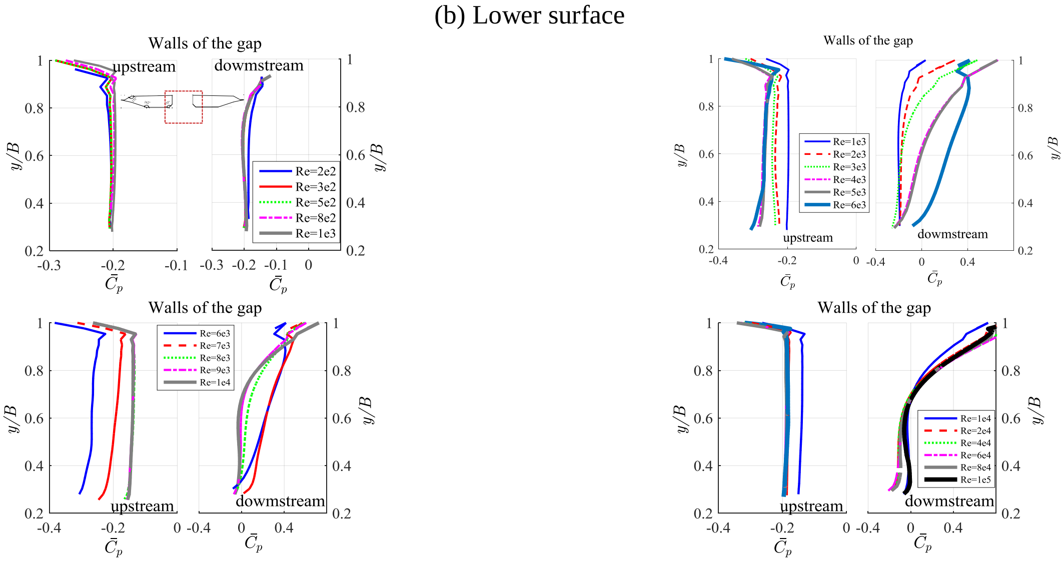

(c) Walls of the gap

Fig. 8 Mean pressure distributions on the surface of twin-box girder at various Reynolds numbers

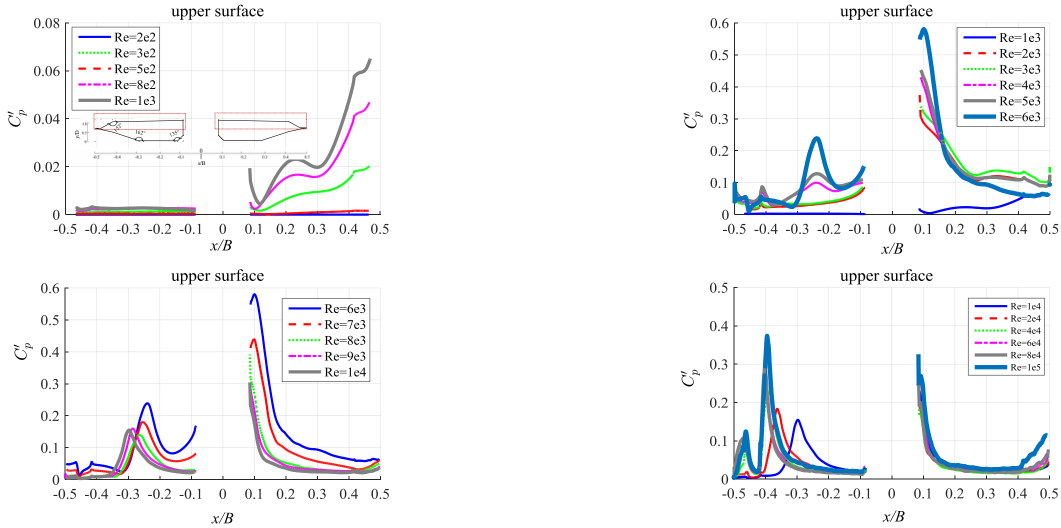

(a) Upper surface

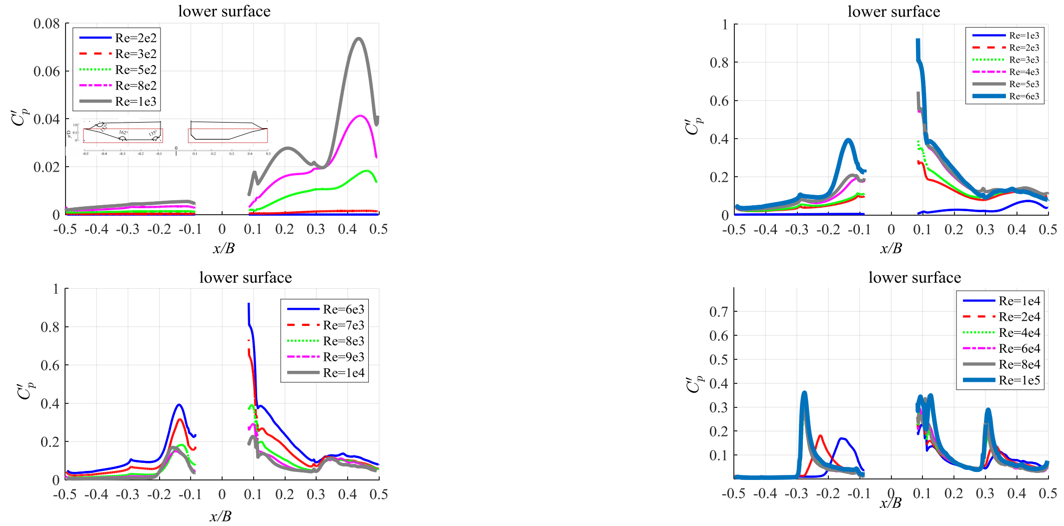

(b) Lower surface

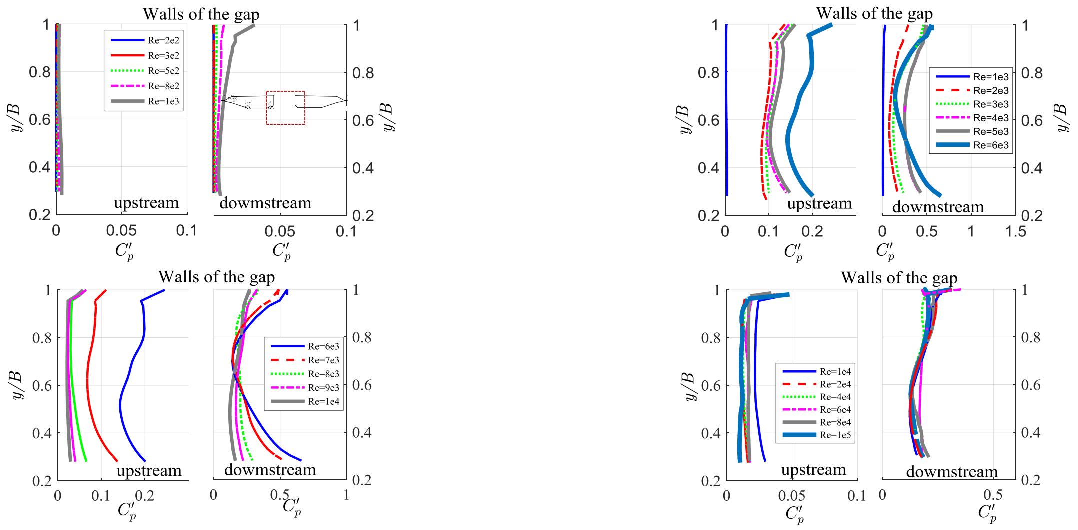

(c) Walls of the gap

Fig. 9 RMS of fluctuating pressure distributions on the surface of twin box girder at various Reynolds numbers

$$C_p = \frac{p - p_\infty}{1/2\rho_{air}U^2} \tag{10}$$

where p is pressure, p_∞ is the pressure of the free stream, and ρ_{air} is the density of air.

Fig. 8 shows the mean pressure coefficient distribution on the surface of the girder model at various Reynolds numbers, while Fig. 9 presents the RMS of fluctuating pressure coefficient distribution at various Reynolds numbers. Both figures indicate clearly that the pressure coefficients have Reynolds number dependence.

As Figs. 8 and 9 show, at the leading edges of the upstream box girder, the pressures present significant Reynolds number sensitivity. For low Reynolds numbers (Re ≤ 1e3), as the viscous force is dominant, the flow attaches onto the surface of the upstream box girder. Therefore, the pressure coefficient distribution almost remains the same in this Reynolds number range. For 1e3 < Re ≤ 5e3, the laminar flow separates slightly in the vicinity of the windward corner (Corner A and B), and then reattaches onto the surface by forming a laminar separation-laminar reattachment bubble (see Fig. 8), which induces a slight decrease in the adverse pressure gradient. As the Reynolds number further increases (6e3 ≤ Re ≤ 8e4), the separation angle increases, and a laminar separation-turbulent reattachment state occurs. Usually, the pressures in the separation region almost remain the same at the separation point. As the very weak shear stresses operate in the region (see Fig. 10, where shows the shin-friction distribution on the upper surface of upstream box girder at Re = 6e3), the shear layer does not have the ability to withstand a large pressure gradient (Horton 1968). However, as the separated shear layer transits to turbulence with a high adsorption capacity, the large negative peak shin friction appears, as shown in Fig. 10, causing the pressure to recover again. Therefore, a pressure plateau region exists in the upstream portion of the separation region. Moreover, the shear-layer is highly unsteady, with shedding vortex impingement on its surface in the laminar separation-turbulent reattachment state, which causes a large peak in surface-pressure fluctuation (Fig. 10). This feature has been observed in many studies (Cherry *et al.* 1984, Kiya and Sasaki 1983, 1985, Lee and Sung 2001, Chun *et al.* 2004). As Fig. 10 shows, the maximum surface-pressure fluctuation point and the maximum negative skin friction point are located between the termination of the pressure plateau and the reattachment point. Furthermore, the maximum surface-pressure fluctuation is located downstream of the maximum negative skin friction. The stream-wise locations of termination of the pressure plateau, the maximum negative skin friction point, and the maximum surface-pressure fluctuation point at Re = 6e3 are as follows: $(x_t - x_s)/l_b$ = 0.7697, $(x_{c_f\text{-peak}} - x_s)/l_b$ = 0.8449, and $(x_{c_p\text{-peak}} - x_s)/l_b$ = 0.9447. In this study, the location of zero skin friction is considered as a separation point when the skin friction coefficient turns from positive to negative. However, when the skin friction coefficient becomes positive, the location of zero skin friction is then considered as a reattachment point. Fig. 11 highlights the relationships between the Reynolds number and termination of the pressure plateau, the location of maximum surface-pressure fluctuation, and the reattachment point. For the separated shear layer, the turbulence transition point gradually moves upstream with an increase in Reynolds number, which causes the pressure plateau termination and reattachment point to also moves upstream, i.e., the width of the pressure plateau and length of the separated bubble gradually decrease. However, the negative pressure value (suction) of the plateau increases with an increase in the Reynolds number, as shown in Fig. 12. It is worth noting that the adverse pressure gradient is almost the same at various Reynolds numbers in the pressure recovery region. At sufficiently high Reynolds numbers (Re > 8e4), the leading laminar boundary layer transits to turbulence, and the turbulent flow slightly separates in the vicinity of the windward corner (Corner A and B), causing the pressure to recover rapidly. In this Reynolds number range, the pressure distribution varies little with the Reynolds number, except at the leading separation point, where the suction increases with increases in the Reynolds number.

Around the gap, the pressures also have Reynolds number sensitivity, as the gap flow pattern varies with the Reynolds number, as shown in Figs. 8 and 9.

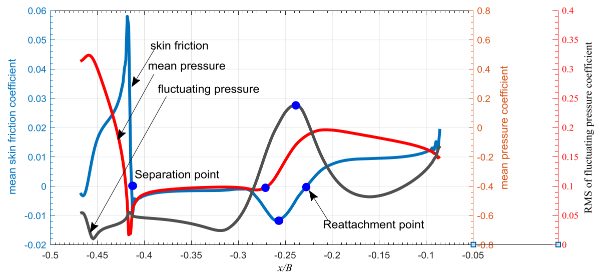

Fig. 10 Mean skin-friction coefficient on the upper surface of upstream box girder at Re=6e3

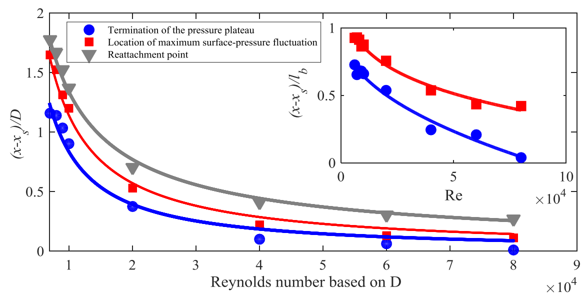

Fig. 11 Termination of the pressure plateau and the location of the maximum surface-pressure fluctuation against the Reynolds number (x_s is x-direction location of separation point, l_b is bubble length)

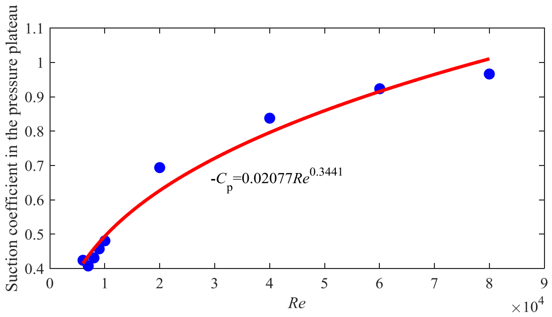

Fig. 12 Relationship between the suction coefficient of pressure plateau and the Reynolds number

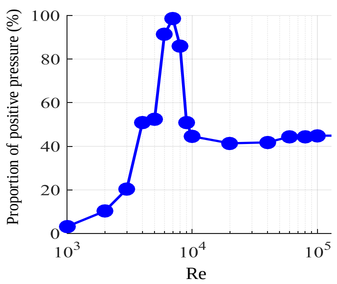

Fig. 13 Relationship between the proportion of positive pressures on the downstream wall of the gap and the Reynolds number

For Re ≤ 1e3, the incoming flows directly cross the gap, and the gap flow is stable, i.e., the mass exchange between the incoming flow from the upstream box girder and the gap flow is very weak. Both of the pressures on the upstream and downstream walls of the gap are negative, and do not vary with the Reynolds number. For 1e3 < Re < 5e3, because of K-H instability of the upper and lower shear layers, the K-H vortices form in the gap and impinge on the corners (Corner G and H) when traveling downstream, resulting in large pressure fluctuations in the vicinity of the corners. Furthermore, the portion of positive pressure on the wall gradually increases as the Reynolds number increases (Fig. 13 presents the proportion of positive pressure as a function of Reynolds number). For Re in the range 6e3–8e3, strong alternately shedding Karman-like vortices induced by the interaction of the upper and lower shear layers are generated in the gap and impinge on the downstream wall of the gap when traveling downstream. Under the effect of alternately shedding Karman-like vortices, the pressures on the entire downstream wall of the gap become positive and show significant fluctuations. Furthermore, the pressures at the downstream of the corners (Corner G and H) display considerable suctions with adverse pressure gradients. For Re > 8e3, as the interaction between the upper and lower shear layers becomes weaker owing to the effect of incoming turbulence, the alternately shedding Karman-like vortices gradually break into small vortices in the gap, inducing a decrease in the pressure fluctuation on the walls, and approximate 60% of the pressures on the downstream wall of the gap become negative. In this Reynolds number range, the pressure distributions on the walls of the gap do not have an obvious tendency with the Reynolds number

At the trailing edges of the downstream box girder, the pressure distributions correlate with the wake dynamics. For lower Reynolds number (3e2 ≤ Re ≤ 1e3), vortex-induced pressure fluctuations increase with an increase in the Reynolds number as a result of the Karman vortex gradually approaching the base of the downstream box girder. For Re >1e3, as the lower separation shear layer transits to turbulence, the flow on the lower side reattaches onto the lower-trailing edge, and the reattachment point gradually moves upstream as the Reynolds number increases. The lower separation region gradually shrinks until Re = 6e4, as shown in Fig. 14, which shows the mean streamlines in the tail of the twin-box girder at various Reynolds number. Owing to the reattachment of the flow on the lower side, the pressures on the lower trailing edge gradually recover with an increase in the Reynolds number. As the reattachment point moves upstream and the separation region shrinks, the position of maximum RMS of fluctuating pressure also moves upstream, and the maximum suction on the lower-trailing edge increases.

3.3 Reynolds number effects on aerodynamic forces

The aerodynamic force coefficients are defined as

$$C_d = \frac{F_d}{\frac{1}{2}\rho_{air}U_\infty^2 Dl} \tag{11}$$

$$C_l = \frac{F_l}{\frac{1}{2}\rho_{air}U_\infty^2 Bl} \tag{12}$$

$$C_m = \frac{F_m}{\frac{1}{2}\rho_{air}U_\infty^2 B^2 l} \tag{13}$$

where C_d, C_l, C_m are the drag, lift, and moment force coefficient, respectively; F_d, F_l, F_m are the drag, lift, and moment force respectively; D is height of the twin-box girder; B is the width of model; and l is the length of the model.

The mean and fluctuating aerodynamic force coefficients of the girder at various Reynolds numbers are shown in Figs. 15 and 16, respectively. For Re ≤ 1e3, the time-averaged drag force coefficient decreases as the Reynolds number increases, while the mean lift and moment force coefficients do not have obvious Reynolds number dependence. In this range, the sensitivity of the drag force to the Reynolds number is mainly due to the reduction in the viscous force coefficients on the surfaces, as Fig. 15(d) shows. Moreover, the fluctuating lift force coefficient shows a slight increasing tendency that is induced by the Karman shedding vortex gradually approaching the base of the downstream box girder. For 1e3 < Re ≤ 8e3, the mean and fluctuating aerodynamic force coefficients show significant variations with the Reynolds number that are associated with the

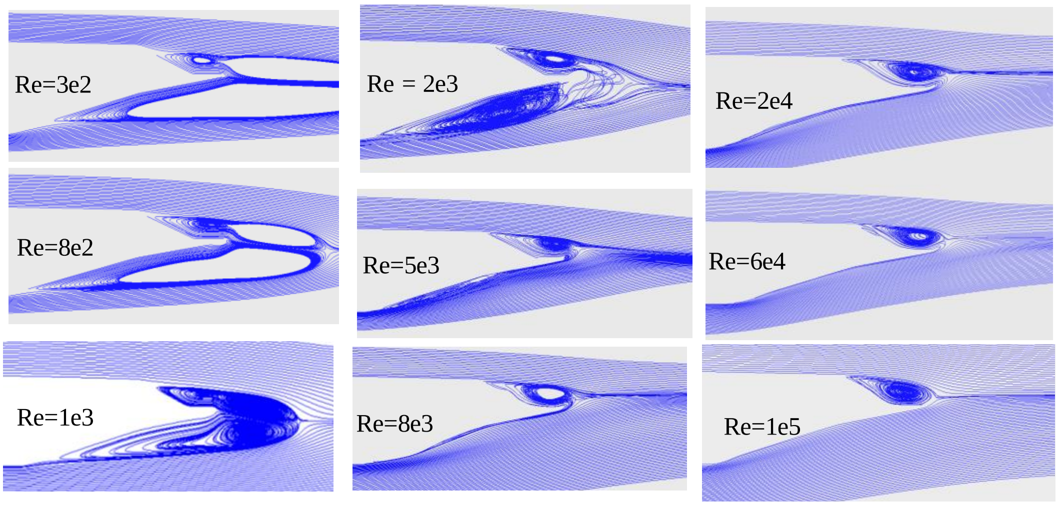

Fig. 14 Mean streamlines around the trailing edges at various Reynolds numbers

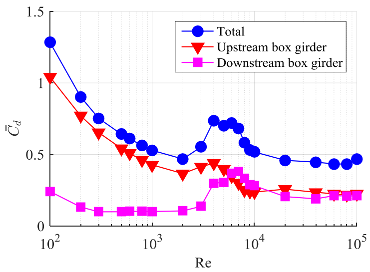

(a) Drag force coefficient

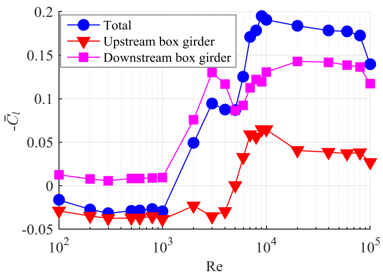

(b) Lift force coefficient

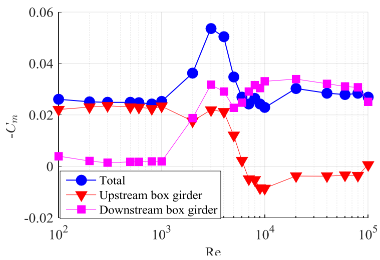

(c)Moment force coefficient

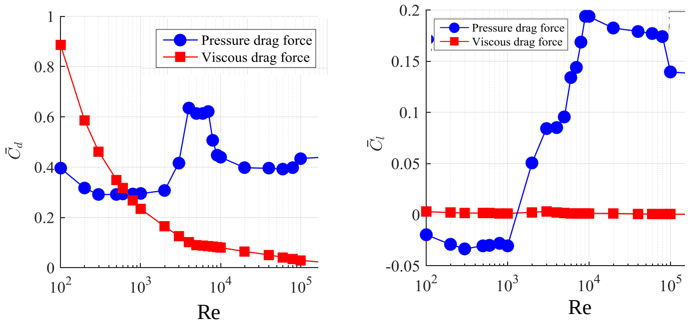

(d) Viscous and pressure force coefficients

Fig. 15 Relationship between mean aerodynamic force coefficients and the Reynolds number

instability and the interaction strength of the upper and lower shear layers of the gap. At 1e3 < Re ≤ 6e3, the instability of shear layers and the interaction strength of the upper and lower shear layers of the gap increases, which induces a K-H vortex and large Karman vortex shedding in the gap, causing the flows to separate around the windward corner (Corner G and H) of the downstream box girder; thus, the mean and fluctuating aerodynamic force coefficients show a significant increasing tendency. At 6e3 < Re ≤ 8e3, owing to the turbulence disturbance of the upstream flow, the strength of the interaction between the upper and lower shear layers of the gap decreases; therefore, the mean and fluctuating aerodynamic force coefficients show a decrease tendency. However, it should be noted that the time-averaged lift force coefficient increases with the increase in the Reynolds number, as the suctions gradually increase on the lower leading edge (see Fig. 15 (b)). At higher Reynolds number (Re > 8e3), the mean lift and moment force coefficients show a decrease tendency with the Reynolds number, which is due to the decrease in the strength of flow separations as the Reynolds number increases, i.e., the flow more easily reattaches on the surface at higher Reynolds number. However, the mean drag force coefficient varies little with the Reynolds number. For the fluctuating forces, they do not show an obvious tendency with the Reynolds number.

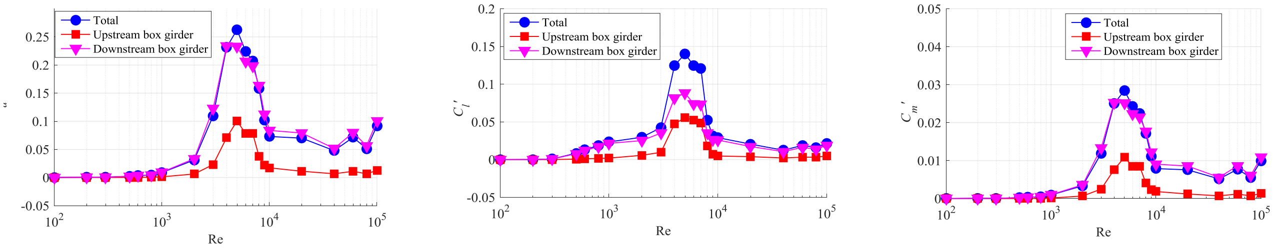

(a) Fluctuating drag force coefficient (b) Fluctuating lift force coefficient (c) Fluctuating moment force coefficient

Fig. 16 Relationship between fluctuating aerodynamic force coefficients and the Reynolds number

5. Conclusions

The Reynolds number effects on the flow characteristics of a twin-box girder were investigated by LES with Reynolds numbers located in the range 1e2 ≤ Re ≤ 1e5 based on the height of the twin-box girder. The conclusions are as follows:

As the flows gradually become unstable and transform into turbulence with an increase in the Reynolds number, the pressure distributions on the surfaces of the stationary twin-box girder show significant Reynolds number dependence, especially in the leading separation region, the impinging region in the downstream wall of the gap, and at the trailing edge of the twin-box girder. Moreover, the aerodynamic forces also show obvious Reynolds number sensitivity.

At the leading edge, the laminar flow separates in the vicinity of the windward corner (Corner A and B) under the adverse pressure gradient at a certain Reynolds number. However, the separating shear layer quickly transitions into turbulence, forcing the turbulence shear layer to reattach onto the surface, which induces the formation of a pressure plateau in the leading edge. Moreover, with the transition point moving upstream, the pressure plateau gradually shrinks, and the location of maximum pressure fluctuation moves close to the termination of the plateaus with an increase in the Reynolds number.

Around the gap, the pressures also have Reynolds number sensitivity associated with the gap flow pattern varying with the Reynolds number. The gap flow goes through complicated flow motions, such as the laminar cavity flow, wake with alternate shedding vortices, and turbulent cavity flow stages in sequence as the Reynolds number increases. For Re ≤ 1e3, the gap flow resembles laminar closed cavity flow, with the upstream shear layers directly crossing the gap; therefore, the pressures are small and stable in the gap. For 2e3 ≤ Re ≤ 8e3, owing to the instability of the shear layers on the upper and lower sides of the gap, which induces the K-H vortices and Karman-like vortices, and the impingement process between vortices and the downstream wall of the gap, the pressures show large fluctuations and high suctions around the downstream wall of the gap. At Re > 8e3, the pressures on the walls of the gap are relatively stable and change very little with the Reynolds number.

At the trailing edge, because the flow undergoes wake instability, the shear layers transition with an increase in the Reynolds number, and the pressures show a corresponding variation with the Reynolds number. In the wake instability region (3e2 ≤ Re ≤ 1e3), the Karman vortex is generated and gradually moves towards the base of the downstream box girder, which causes pressure fluctuations at the trailing edge to increase as the Reynolds number increases. In the shear layer transition stage, because of the strong adsorption ability of turbulence, the separated flows reattach onto the trailing edges, causing that the pressures to recover rapidly.

The characteristics of the leading separation bubble, the gap flow, and the wake flow also have significant effects on the aerodynamic forces. Owing to the unsteady gap flow and the impingement of vortices on the downstream wall of the gap in the range 1e3 < Re ≤ 6e3, the time-averaged and fluctuating aerodynamic force coefficients show a tendency to increase. However, owing to the disturbance of upstream turbulence, the large Karman-like vortex become smaller, which causes the time-average and fluctuating aerodynamic force coefficients to show a decreasing tendency in the range 6e3 < Re ≤ 8e3, except the time-averaged lift force, which shows an opposite tendency that is due to an increase in suctions on the lower leading edge. As the Reynolds number further increases, Re > 8e3, the drag force coefficient shows little variation with the Reynolds number, while the time-averaged lift force has a decreasing tendency.

Acknowledgments

The study was supported by the NSFC (51503138), the China Postdoctoral Science Foundations (2015M580266 and 2016T90295), the Heilongjiang Postdoctoral Fund (LBH-Z15087), and the Fundament Research Funds for the Central Universities (HIT. NSRIF. 2017064.) The authors acknowledge the use of UCL's Grace High Performance Computing Facility (Grace@UCL), and its associated support services, in the completion of this work. The first author would like to thank Prof. Guoxiong Wu, Dr. Qingchen Meng, Dr. Chongwei Zhang, and Prof. Zhen Wang for their precious discussions and kind help during visits to the Mechanical Department of UCL.

References

Bruno, L. and Khris, S. (2003), "The validity of 2D Numerical simulations of vortical Structures around a bridge deck", *Math. Comput. Model*., **37**(7-8), 795-828. https://doi.org/10.1016/S0895-7177(03)00087-6.

Cherry, N.J., Hillier, R. and Latour, M.E.M.P. (1984), "Unsteady measurements in a separated and reattaching flow", *J. Fluid Mech*, **144**, 13-46. https://doi.org/10.1017/S002211208400149X.

Chun, S., Liu, Y.Z. and Sung, H.J. (2004), "Wall pressure fluctuations of a turbulence separated and reattaching flow affected by an unsteady wake", *Exp. Fluids*, **37**(4), 531-546.

Dragomirescu, E., Wang, Z. and Hoftyzer, M.S. (2016), "Aerodynamic characteristics investigation of megane multi-box bridge deck by CFD-LES simulations and experimental tests", *Wind Struct.*, **22**(2), 161-184. https://doi.org/10.12989/was.2016.22.2.161.

Germano, M., Piomelli, U., Moin, P. and Cabot, W.H. (1991), "A dynamic subgrid-scale eddy viscosity model", *Phys. Fluid. A: Fluid Dynam.*, **3**(7), 1760-1765. https://doi.org/10.1063/1.857955.

Horton, H.P. (1968), "Laminar separation in two and three-dimensional incompressible flow", PhD Dissertation, University of London, London.

Kargarmoakhar, R., Chowdhury, A.G. and Irwin, P.A. (2015), "Reynolds number effects on twin box girder long span bridge aerodynamics", *Wind Struct.*, **20**(2), 327-347. https://doi.org/10.12989/was.2015.20.2.327.

Kiya, M. and Sasaki, K. (1983), "Structure of a turbulent separation bubble", *J. Fluid Mech.*, **137**, 83-113. https://doi.org/10.1017/S002211208300230X.

Kiya, M. and Sasaki, K. (1985), "Structure of. large-scale vortices and unsteady reverse flow in the reattaching zone of a turbulent separation bubble", *J. Fluid Mech.*, **154**, 463-491. https://doi.org/10.1017/S0022112085001628.

Kuroda, S. (1997), "Numerical simulation of flow around a box girder of a long span suspension bridge", *J. Wind Eng. Ind. Aerod*., **67-68**, 239-252. https://doi.org/10.1016/S0167-6105(97)00076-7.

Laima, S., Jiang, C., Li, H., Chen, W. and Ou, J. (2018), "A numerical investigation of Reynolds number sensitivity of flow characteristics around a twin-box girder", *J. Wind Eng. Ind. Aerod*., **172**, 298-316. https://doi.org/10.1016/j.jweia.2017.11.016.

Larose, G.L. and D'Auteuil, A. (2006), "On the Reynolds number sensitivity of the aerodynamics of bluff bodies with sharp edges", *J. Wind Eng. Ind. Aerod*., **94**(5), 365-376. https://doi.org/10.1016/j.jweia.2006.01.011.

Larsen, A. and Walter, J.H. (1997), "Aeroelastic analysis of bridge girder sections based on discrete vortex simulations", *J. Wind Eng. Ind. Aerod*., **67-68**, 253-265. https://doi.org/10.1016/S0167-6105(97)00077-9.

Larsen, A., Savage, M., Lafrenière, A. and Larsen, S.V. (2008), "Investigation of vortex response of a twin box bridge section at high and low Reynolds numbers", *J. Wind Eng. Ind. Aerod*., **96**(6), 934-944. https://doi.org/10.1016/j.jweia.2007.06.020.

Lee, D., Kawai, S., Nonomura, T., Anyoji, M., Aono, M., Oyama, A., Asai, K., and Fujii, K. (2015), "Mechanism of surface pressure distribution within a laminar separation bubble at different Reynolds numbers", *Phys. Fluids.*, **27**(2), 023602-1-22. https://doi.org/10.1063/1.4913500.

Lee, I. and Sung, H.J. (2001), "Characteristics of wall pressure fluctuations in separated and reattaching flows over a backward-facing step: part 1. Time-mean statistics and cross-spectral analyses", *Exp. Fluids.*, **30**(3), 262-272.

Li, H., Laima, S.J. and Jing, H.Q. (2014), "Reynolds number effects on aerodynamic characteristics and vortex-induced vibration of a twin-box girder", *J. Fluid. Struct.*, **50**, 358-375. https://doi.org/10.1016/j.jfluidstructs.2014.06.027.

Lilly, D.K. (1992), "A proposed modification of the germane subgrid-scale closure model", *Phys. Fluid. A: Fluid Dynam.*, **4**(3), 633-635. https://doi.org/10.1063/1.858280.

Liu, Z.L., Kang, W. and Sung, H.J. (2005), "Assessment of organization of a turbulent separated and reattaching flow by measuring wall pressure fluctuations", *Exp. Fluids*, **38**(4), 485-493

Mannini, C., Soda, A., VoB, R. and Schewe, G. (2010), "Unsteady RANS simulation of flow around a bridge section", *J. Wind Eng. Ind. Aerod*., **98**(12), 742-753. https://doi.org/10.1016/j.jweia.2010.06.010.

Miranda, S.D, Patruno, L, Ricci, M. and Ubertini, F. (2015), "Numerical study of a twin box bridge deck with increasing gap ratio by using RANS and LES approaches", *Eng. Struct.*, **99**, 546-558. https://doi.org/10.1016/j.engstruct.2015.05.017.

Nicoud, F. and Ducros, F. (1999), "Subgrid-Scale stress modelling based on the square of the velocity gradient tensor", *Flow Turbul.Combust.*, **62**(3), 183-200

Nieto, F., Hernandez, S., Jurado, J.A. and Baldomir, A. (2010), "CFD practical application in conceptual design of a 425 m cable-stayed bridge", *Wind Struct.*, **13**(4) 309-326. https://doi.org/10.12989/was.2010.13.4.309.

Norberg, C. (2003), "Fluctuating lift on a circular cylinder: Review and new measurements", *J. Fluid. Struct.*, **17**(1), 57-96. https://doi.org/10.1016/S0889-9746(02)00099-3.

Ota, T., Asano, Y. and Okawa, J. (1981), "Reattachment length and Transition of the separated flow over bluff flat plates", *Bulletin JSME*, **24**(192), 941-947. https://doi.org/10.1299/jsme1958.24.941.

Sasaki, K. and Kiya M. (1991), "Three-dimensional vortex structure in a leading-edge separation bubble at moderate Reynolds numbers", *J. Fluid. Eng.*, **113**(3), 405-410. doi:10.1115/1.2909510.

Schewe, G. (2001), "Reynolds number effects in flow around more-or-less bluff bodies", *J. Wing Eng*., **89**, 1267-1289.

Schewe, G. and Larsen, A. (1998), "Reynolds number effects in the flow around a bluff bridge deck across section", *J. Wind Eng. Ind. Aerod.*, **74-76**, 829-838. https://doi.org/10.1016/S0167-6105(98)00075-0.

Wang, X. and Gu, M. (2015), "Experimental investigation of Reynolds number effects on 2d rectangular prisms with various side ratios and rounded corners", *Wind Struct.*, **21**(2), 183-202. https://doi.org/10.12989/was.2015.21.2.183.

Watanabe, S. and Fumoto, K. (2008), "Aerodynamic study of slotted box girder using computational fluid dynamics", *J. Wind Eng. Ind. Aerod*., **96**(10-11), 1885-1894. https://doi.org/10.1016/j.jweia.2008.02.056.

Williamson, C.H.K. (1996), "Vortex dynamics in the cylinder wake", *Annu. Rev. Fluid. Mech*., **28**, 477-539. https://doi.org/10.1146/annurev.fl.28.010196.002401.

Yang, Z. and Voke, P.R. (2001), "Large-eddy simulation of boundary-layer separation and transition at a change of surface curvature", *J. Fluid. Mech.*, **439**, 305-333. https://doi.org/10.1017/S0022112001004633.

Zdravkovich, M.M. (1997), Flow around circular cylinders Volume 1: Fundamentals, Oxford Science Publications, USA

Zhang, W., Ge, Y.J., Wei, Z.G. and Yang, Y.X. (2008), "Experiments on vortex induced vibration of twin-box bridge sections in high and low Reynolds numbers", *Acta Aerod. Sin*, **26**(3), 356-359 (in Chinese).

Zhou, Z. and Ma, R. (2010), "Numerical simulation study of the Reynolds number effect on two bridge decks based on the deterministic vortex method", *Wind Struct*., 1**3**(13), 347-362. https://doi.org/10.12989/was.2010.13.4.347.

CC